

Wave breaking in tapered holey fibers

Shuguang Li (李曙光)^{1,2*}, Lei Zhang (张磊)¹, Bo Fu (付博)¹, Yi Zheng (郑义)²,
Ying Han (韩颖)¹, and Xingtao Zhao (赵兴涛)^{1,2}

¹Key Laboratory of Metastable Materials Science and Technology, College of Science,
Yanshan University, Qinhuangdao 066004, China

²School of Science, Beijing Jiaotong University, Beijing 100044, China

*Corresponding author: shuguangli@ysu.edu.cn

Received July 20, 2010; accepted November 15, 2010; posted online February 21, 2011

We numerically study the propagation of 1-ps laser pulse in three tapered holey fibers (THFs). The curvature indices of the concave, linear, and convex tapers are 2.0, 1.0, and 0.5, respectively. The central wavelength, located in the normal dispersion regime, is 800 nm. The nonlinear coefficient of the THFs increases from the initial $0.095 \text{ m}^{-1} \cdot \text{W}^{-1}$ to the final $0.349 \text{ m}^{-1} \cdot \text{W}^{-1}$. Wave breaking accompanied by oscillatory structures occurs near pulse edges, and sidelobes appear in the pulse spectrum. With the increase in propagation distance z , the pulse shape becomes broader and the pulse spectrum flattens. A concave THF is advantageous to the generation of wave breaking and enables easier achievement of super flat spectra at short lengths.

OCIS codes: 060.2310, 060.4370, 060.2270.

doi: 10.3788/COL201109.030601.

Holey fibers (HFs), which are also known as microstructure optical fibers (MOFs) or photonic crystal fibers (PCFs), have recently attracted increasing interest. A HF is typically a single-material-based optical fiber with air-filled holes that surround the core area and can provide strong mode confinement to light field^[1–3], long interaction lengths, and customizable wavelength dispersion^[4,5]. A HF is a suitable nonlinear medium for the observation of a wide variety of nonlinear effects at low power^[6,7]. Furthermore, HFs with high nonlinear coefficients are suitable for manufacturing fiber devices such as amplifiers, switches, gratings, and so on^[8].

Tapered holey fibers (THFs) are powerful post-processing techniques for adjusting the properties of a given section of a HF. The tapering process enhances nonlinearity by reducing core size^[9,10]. More efficient nonlinear devices can be obtained. Mägi *et al.* reported a THF that achieved a microstructural pitch of less than 300 nm^[11] and Xu *et al.* numerically studied supercontinuum generation in a THF with flattened dispersion properties^[12].

The propagation of ultrashort laser pulse in HFs is described by the nonlinear Schrödinger equation. Both group velocity dispersion (GVD) and nonlinear effects play significant roles during pulse propagation^[13]. Anderson *et al.* propose that in a normal dispersion regime, the combination of GVD and nonlinear effects makes a strong-intensity pulse broaden and changes the shape of the pulse into an almost rectangular form. This evolution can be understood as being caused by frequency chirp, which is induced by GVD and self-phase modulation. However, the evolution is also accompanied by the appearance of oscillation in the wings of the pulse and sidelobes on the pulse spectrum. These features are interpreted as being created when the shifted light overruns the pulse; then, the pulse contains light at two different frequencies, which interfere and generate new frequencies^[14]. The suggested term for this phenomenon

is optical wave breaking^[15].

In this letter, we numerically simulate the propagation of a laser pulse using the adaptive split-step Fourier method. The pulse has a width of 1 ps and a central wavelength of 800 nm in a uniform HF and three THFs with regular triangular formations.

In the numerical simulation, the equation that describes the parameters of the THFs is expressed as^[16]

$$\Lambda(z) = \Lambda_b + (\Lambda_b - \Lambda_s) \left[\left(1 - \frac{z}{l} \right)^\eta - 1 \right], \quad (1)$$

where $\Lambda(z)$ is the pitch of the air holes of the THF at distance z ; Λ_b and Λ_s are the pitches of the air holes at the thick and thin ends of the THF, respectively; z is the distance to the thick end in the Cartesian coordinate system; η represents the curvature index; l denotes the total length of the THF. In this letter, $\Lambda_b = 1.0 \mu\text{m}$, $\Lambda_s = 0.4 \mu\text{m}$, and $l = 0.2 \text{ m}$. At the thick end, the diameter of the air hole is $0.5 \mu\text{m}$, whereas that at the thin end is $0.2 \mu\text{m}$. The air filling fraction is maintained at 25%. Figure 1(a) shows the shape of the THFs and (b) shows the variation in pitch Λ with distance z , with curvature indices η at 0.5, 1.0, and 2.0, respectively. The variation in the core diameter with distance z is the same as that of pitch. When curvature index $\eta = 1.0$, the variation is linear. When $\eta = 0.5$, the shape of the THF is convex, whereas when $\eta = 2.0$, the shape of the THF is concave.

The input laser pulse is an initially non-chirped hyperbolic-secant pulse^[4] with a central wavelength of 800 nm. The optical field often takes the form of $A(0, T) = \sqrt{P_0} \text{sech} h \left(\frac{T}{T_0} \right)$, where P_0 is the peak power of the input pulse, T is the time parameter of the frame moving with the pulse at the group velocity, and T_0 denotes the half-width of the input pulse. In practice, it is customary to use the full width at half maximum (FWHM) in place of T_0 . In this letter, $P_0 = 3.809 \text{ kW}$, and $\text{FWHM} = 1.763T_0 = 1 \text{ ps}$. Although peak power P_0 is large and the fiber length is short, the parameters

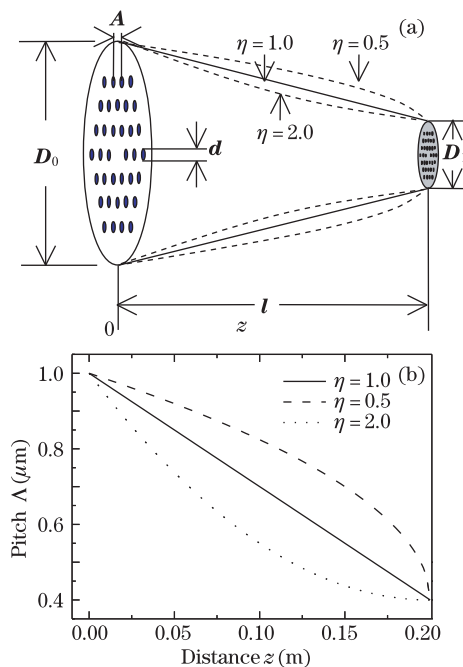


Fig. 1. (a) Shape of THFs; (b) variation in pitch with distance z in THFs.

of the THF vary more largely along the axes of the fiber so that the confinement loss can be considered using the adaptive split-step Fourier method.

Figure 2(a) shows the nonlinear coefficient at a wavelength of 800 nm as a function of distance z . The nonlinear coefficient increases and the core diameter decreases with increasing distance z . Meanwhile, the mode area becomes small as a result of the increase in confinement. The nonlinear coefficients at the thick and thin ends of the THF are 0.095 and $0.349 \text{ m}^{-1} \cdot \text{W}^{-1}$, respectively. Comparing the nonlinear coefficients of the three THFs, we know that for the same distance z , the nonlinear coefficient of the concave THF with curvature index $\eta = 2.0$ is always the largest. Figure 2(b) shows the second-order dispersion coefficient at a wavelength of 800 nm as a function of distance z . The input pulse is in the normal dispersion regime for the three THFs. In the simulation of this letter, calculated dispersion coefficients reach the 15th order.

Figure 3 shows the pulse shape evolution of the initially non-chirped hyperbolic-secant pulse with a wavelength of 800 nm, located in the normal dispersion regime. The uniform HF and the three THFs both have regular triangular formations. In the uniform HF, the pitch of the air holes is $1.0 \mu\text{m}$ and the diameter of each air hole is $0.5 \mu\text{m}$. Figure 3(a) shows fast oscillatory structures present in the pulse shape; the peak power of the pulse increases and sub-pulses are formed, with the propagation of laser pulse inside the uniform HF. The sub-pulses increase with increasing transmission distance and have approximately the same interval, width, and amplitude. For the THFs, the peak power of the pulse decreases with increasing propagation distance. As shown in Fig. 3(b), the curvature of the linear THF is 1.0, with slight oscillation present near the pulse edge at $z = 16 \text{ cm}$. This indicates that wave breaking occurs near $z = 16 \text{ cm}$. At $z = 20 \text{ cm}$, the oscillatory structures are clearer and the

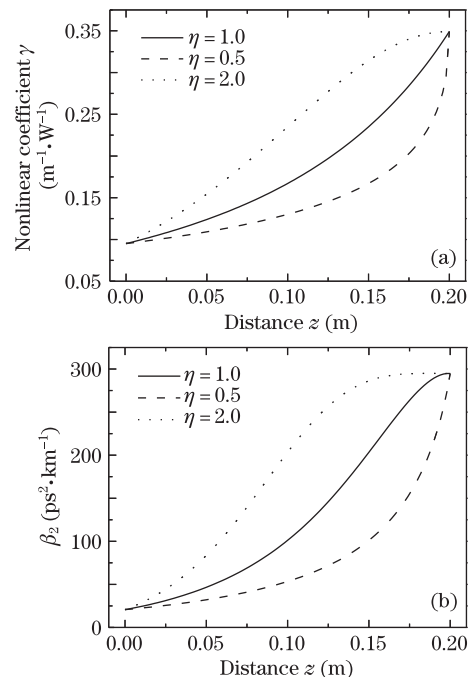


Fig. 2. (a) Nonlinear coefficient and (b) the second-order dispersion at a central wavelength of 800 nm as a function of distance z .

pulse shape is broader, demonstrating that the degree of wave breaking increases and the oscillatory extent of the pulse is amplified. The oscillation near pulse edges is a sign of wave breaking. For the convex and concave THFs, whose curvatures are 0.5 and 2.0, respectively, the oscillation structures at $z = 20 \text{ cm}$ and $z = 12 \text{ cm}$ are shown in Figs. 3(c) and (d). The distance of wave breaking in the THF is determined by dispersion length and nonlinear length. The dispersion length and nonlinear length can be adjusted using the THFs and laser pulse with different parameters. Thus, the wave breaking distance can be modified. Further increases in z can lead to the broadening of the pulse tails. Comparing the wave breaking distance in the three THFs, we know that the wave breaking distance of the concave THF, whose curvature $\eta = 2.0$, is the shortest.

Figure 4 shows the pulse spectrum evolution of an initially non-chirped hyperbolic-secant pulse with a wavelength of 800 nm. As shown in Fig. 4(a), with the propagation of the pulse, the frequency spectrum of the pulse presents periodic variation in the uniform HF. The spectra broaden at $z = 8 \text{ cm}$, narrow down at $z = 12 \text{ cm}$, and broaden again at $z = 20 \text{ cm}$. With the propagation of the pulse in the THFs, the pulse spectrum widens and is accompanied by an oscillatory structure that consists of many peaks covering the entire frequency range. Figure 4(b) shows that the pulse spectrum exhibits obvious sidelobes at $z = 16 \text{ cm}$ in the linear THF whose curvature is 1.0. Further increase in z can lead to continuous broadening of the pulse spectrum, rise of the sidelobes, and flattening of the pulse spectrum top. The spectral intensities of the pulse are distributed evenly. For the convex and concave THFs, whose curvatures are 0.5 and 2.0, respectively (Figs. 4(c) and (d)), the pulse spectrum exhibits obvious sidelobes at $z = 20 \text{ cm}$ and $z = 12 \text{ cm}$. The distance of the pulse spectrum exhibiting obvious

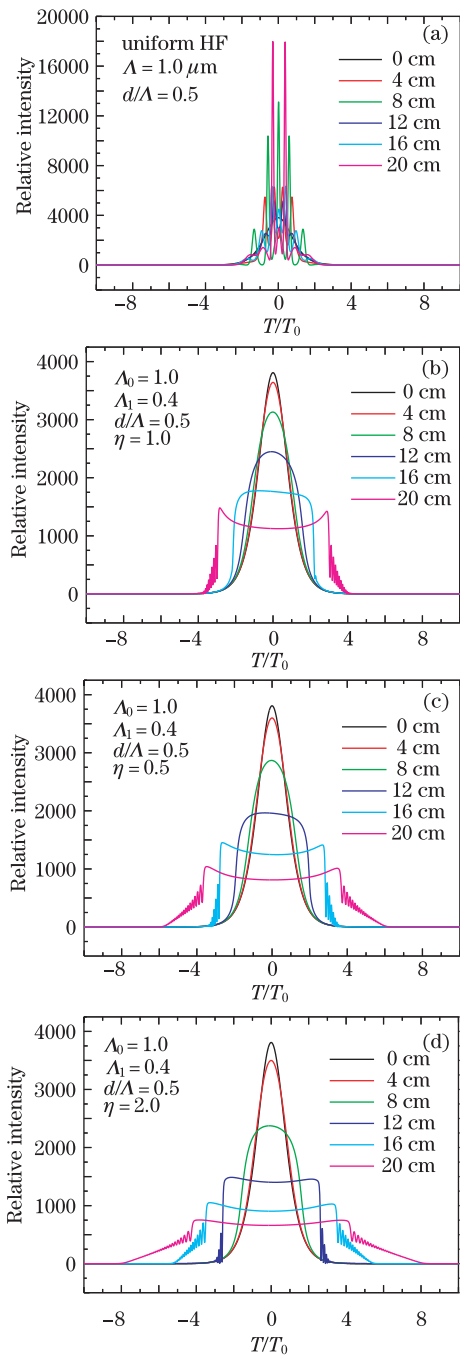


Fig. 3. (a) Evolution of pulse shape in uniform HF and THFs with curvatures of (b) 1.0, (c) 0.5, and (d) 2.0.

sidelobes coincides with that of the pulse shape, which presents oscillatory structures. They are both signs of wave breaking.

Figure 5 shows the pulse spectrum at $z = 20$ cm in the uniform HF whose pitch is $1.0 \mu\text{m}$ and the THFs whose curvatures are 1.0, 0.5, and 2.0, respectively. We can see that in the uniform HF the spectrum is narrower than those of the THFs. THFs are more inclined to spectral broadening. From the spectrum of the THF we can observe considerable energy concentration in the region of central frequency, in which many peaks appear. Sidelobes appear near the edge of the spectrum. For the convex THF whose curvature is 0.5, the region of central frequency where most of the energy is concentrated is the

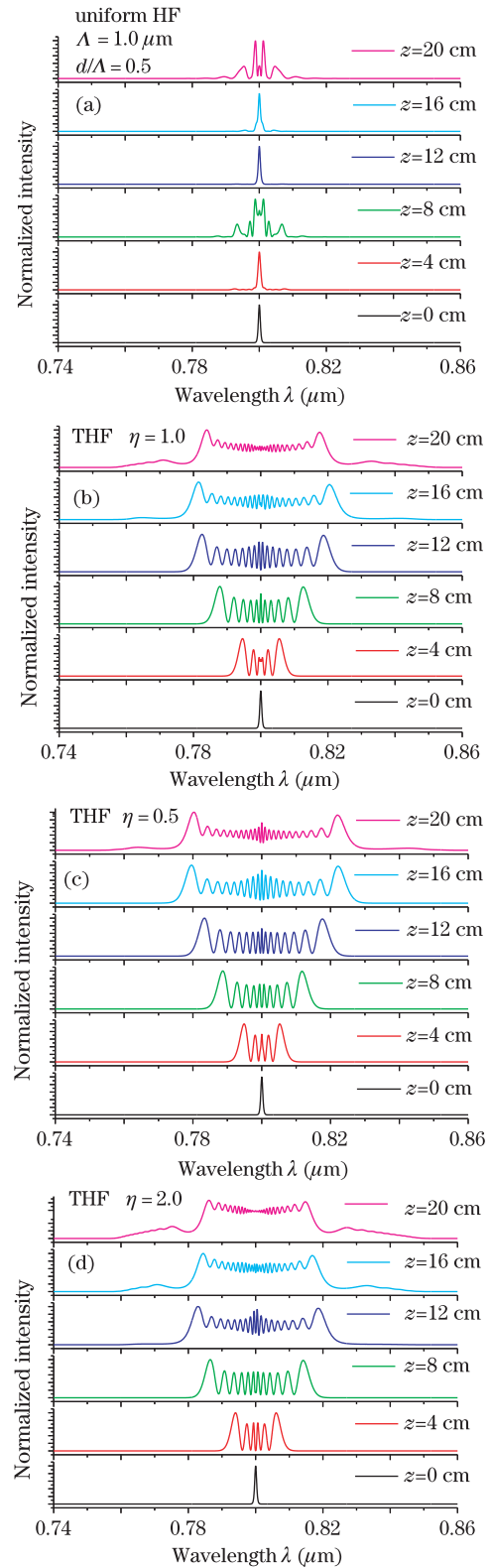


Fig. 4. (a) Evolution of pulse spectrum in uniform HF and THFs with curvatures of (b) 1.0, (c) 0.5, and (d) 2.0.

largest of the three THFs; the sidelobe structure is very small, indicating that only minimal energy is distributed at the edge of the frequency. For the concave THF whose curvature is 2.0, the region where energy is focused on is the smallest of the three THFs. The normalized intensity is close to the largest intensity value and the sidelobe

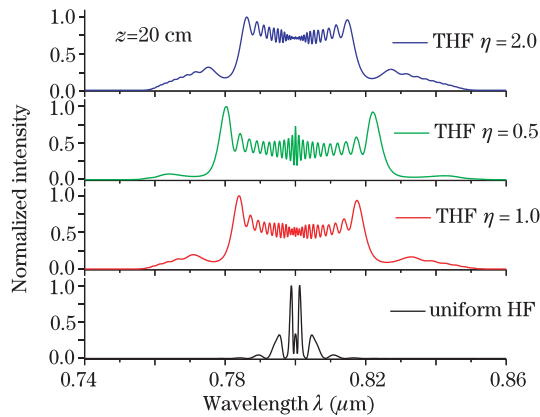


Fig. 5. Pulse spectra at $z = 20$ cm in uniform HF and THFs with curvatures of 1.0, 0.5, and 2.0.

structure is larger than the others. All phenomena indicate that the pulse spectrum is more flattened and the pulse energy is more evenly distributed at the frequency range when the THF is concave. Consequently, a super flat spectrum can be achieved by adjusting the parameters of the THF and laser pulse.

In conclusion, we have numerically studied the propagation of ultrashort laser pulse whose width is 1 ps and wavelength is 800 nm in a uniform HF and three THFs with regular triangular formations. For the uniform HF, the pitch of air holes is $1.0 \mu\text{m}$ and the air hole diameter d is $0.5 \mu\text{m}$. For the THF, the pitches of the air holes at the thick and thin ends are 1.0 and $0.4 \mu\text{m}$, respectively and the curvatures are 2.0, 1.0, and 0.5, respectively. The air filling fraction is maintained at 25%. The nonlinear coefficient increases from the initial $0.095 \text{ m}^{-1}\cdot\text{W}^{-1}$ to the final $0.349 \text{ m}^{-1}\cdot\text{W}^{-1}$. The second-order dispersion coefficients are positive at a wavelength of 800 nm, located in the normal dispersion regime. When the laser pulse propagates in the uniform HF, sub-pulses with high peak power are formed and the frequency spectrum presents periodic variations. When the pulse propagates in the THFs, slight oscillation occurs near pulse edges and the pulse spectrum broadens, accompanied by an oscillatory structure, which leads to wave breaking. For the linear, convex, and concave THFs, the wave breaking distances are 16, 20, and 12 cm, respectively. For the spectrum, the region of energy is the smallest and the normalized intensity is the largest in the concave THF.

Moreover, the sidelobe structure is more obvious. The concave THF is advantageous to wave breaking and enables easier achievement of a super flat spectrum.

This work was supported by the National Natural Science Foundation of China (No. 10874145), the Specialized Research Fund for the Doctoral Program of Higher Education (No. 20091333110010), the Nature Science Foundation of Hebei Province (No. F2009000481), and the China Postdoctoral Science Foundation (Nos. 20080440014 and 200902046).

References

1. T. A. Birks, J. C. Knight, and P. St. J. Russell, *Opt. Lett.* **22**, 961 (1997).
2. J. C. Knight, T. A. Birks, P. St. Russell, and D. M. Atkin, *Opt. Lett.* **21**, 1547 (1996).
3. J. C. Knight, *Nature* **424**, 847 (2003).
4. S. M. Abdur Razzak, Y. Namihira, K. Miyagi, F. Begum, S. Kaijage, N. H. Hai, T. Kinjo, and N. Zou, *Opt. Rev.* **14**, 14 (2007).
5. H. Subbaraman, T. Ling, Y. Jiang, M. Y. Chen, P. Cao, and R. T. Chen, *Appl. Opt.* **46**, 3263 (2007).
6. H. Chen, S. Chen, and J. Hou, *Acta Opt. Sin.* (in Chinese) **30**, 2541 (2010).
7. X. Fang, M. Hu, B. Liu, L. Chai, and Q. Wang, *Chinese J. Lasers* (in Chinese) **37**, 2366 (2010).
8. G. P. Agrawal, *Nonlinear fiber optics*, 3rd ed., (Academic Press, San Diego, 2001).
9. S. Laflamme, S. Lacroix, J. Bures, and X. Daxhelet, *Opt. Express* **15**, 387 (2007).
10. M. Lehtonen, G. Genty, and H. Ludvigsen, *Appl. Phys. B* **81**, 295 (2005).
11. E. Mägi, P. Steinvurzel, and B. Eggleton, *Opt. Express* **12**, 776 (2004).
12. Y. Xu, Z. Chen, H. Li, and Y. Wei, *Frontiers of Optoelectronics in China* **2**, 293 (2009).
13. J. M. Dudley, G. Genty, and S. Coen, *Rev. Mod. Phys.* **78**, 1135 (2006).
14. D. Anderson, M. Desaix, M. Lisak, and M. Quiroga-Teixeiro, *J. Opt. Soc. Am. B* **9**, 1358 (1992).
15. W. J. Tomlinson, R. Stolen, and A. Johnson, *Opt. Lett.* **10**, 457 (1985).
16. E. Khoo, A. Liu, and J. Wu, *Opt. Express* **13**, 7748 (2005).